Chinese Chemical Letters 34 (2023) 107530

Contents lists available at ScienceDirect

Chinese Chemical Letters

journal homepage: www.elsevier.com/locate/cclet

Constructing heterojunction interface of Co_3O_4/TiO_2 for efficiently accelerating acetaminophen degradation *via* photocatalytic activation of sulfite

Qiangwei Li[a], Mengmeng Zhang[a], Yongyi Xu[c], Xiaoqi Quan[a], Yiao Xu[a], Wen Liu[b], Lidong Wang[a,*]

[a] *Department of Environmental Science and Engineering, Hebei Key Lab of Power Plant Flue Gas Multi–Pollutants Control, North China Electric Power University, Baoding 071003, China*
[b] *The Key Laboratory of Water and Sediment Sciences, Ministry of Education, College of Environmental Sciences and Engineering, Peking University, Beijing 100871, China*
[c] *China Power Hua Chuang Electricity Technology Research Company Ltd., Suzhou 215123, China*

ARTICLE INFO

Article history:
Received 14 January 2022
Revised 29 April 2022
Accepted 12 May 2022
Available online 17 May 2022

Keywords:
Sulfite
Photocatalytic activation
Charge transfer
Heterojunction interface
Degradation mechanism

ABSTRACT

Achieving efficient degradation of organic pollutants *via* activation of sulfite is meaningful but challenging. Herein, we have constructed a heterogeneous catalyst system involving Co_3O_4 and TiO_2 nanoparticles to form the p-n heterojunction (Co_3O_4/TiO_2) to degrade acetaminophen (ACE) through photocatalytic activation of sulfite. Specifically, X-ray photoelectron spectroscopy analysis and theoretical calculations provide compelling evidence of electron transfer from Co_3O_4 to TiO_2 at the heterointerface. The interfacial electron redistribution of Co_3O_4/TiO_2 tunes the adsorption energy of HSO_3^-/SO_3^{2-} in sulfite activation process for enhanced the catalytic activity. Owing to its unique heterointerface, the degradation efficiency of ACE reached 96.78% within 10 min. The predominant active radicals were identified as $^{\cdot}OH$, h^+, and $SO_x^{\cdot-}$ through radical quenching experiments and electron spin resonance capture. Besides, the possible degradation pathway was deduced by monitoring the generated intermediate products. Thereafter, the enhanced roles of well-engineered compositing interface in photocatalytic activation of sulfite for complete degradation of ACE were unveiled that it can improve light absorption ability, facilitate the generation of active species, and optimize reactive pathways. Considering that sulfite is a waste from flue gas desulfurization process, the photocatalytic activation of sulfite system will open up new avenues of beneficial use of air pollutants for the removal of pharmaceutical wastewater.

© 2023 Published by Elsevier B.V. on behalf of Chinese Chemical Society and Institute of Materia Medica, Chinese Academy of Medical Sciences.

With water pollution mounting up, sewage treatment has attracted growing attention. Especially, wastewater discharged from hospitals and pharmaceutical industries contains residual drugs that can adversely affect the environment [1]. As a typical non-steroidal anti-inflammatory drug, acetaminophen (ACE) is one of the most commonly used analgesics and antipyretics that has reached the highest detection rate in wastewater and surface water [2,3]. As a result, ACE at different concentrations have been detected in some aquatic organisms. Although the traditional sewage treatment process can effectively remove ACE from wastewater, the process is neither economically nor environmentally friendly. Therefore, the development of novel methods for ACE removal is crucial. Recently, the sulfate radicals-based advanced oxidation (SR-AOPs) has been developed rapidly in sewage treatment, because of its high selectivity and powerful oxidation capacity [3–5]. SR-AOPs can degrade organic compounds by activating some sulfur-containing organic compounds and producing sulfur-oxygen radicals. Thus far, persulfate has been the most commonly used precursor because of its high stability and strong oxidation ability [6,7]; however, it is expensive and can easily produce secondary pollution [8–10]. By contrast, sulfite (S(IV)) as one of the wet flue gas desulfurization (FGD) byproducts is not only cheaper with great production, but also applicable to degrade organic matter [11,12]. Most of the used sulfites can be activated by transition metal compounds and exhibit favorable progress. Chen *et al.* attempted to use Fe(II) species to catalyze sulfite and found that its degradability was comparable to that of activated persulfate and superior to that of a Fenton system [13]. The Fe(0)/Fe(III)-S(IV) system

* Corresponding author.
E-mail address: wld@ncepu.edu.cn (L. Wang).

https://doi.org/10.1016/j.cclet.2022.05.044
1001-8417/© 2023 Published by Elsevier B.V. on behalf of Chinese Chemical Society and Institute of Materia Medica, Chinese Academy of Medical Sciences.

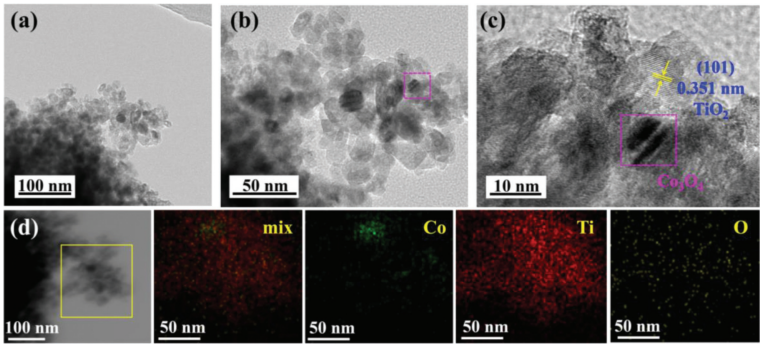

Fig. 1. (a, b) TEM images, and (c) HRTEM image of Co_3O_4/TiO_2. (d) EDS mapping elements.

is well-performed for pollutant degradation under weak acid conditions [14,15]. Although the acidic environment is conducive to the survival of the Cr(VI)-S(IV)-O_2 system [16], Cr(VI) can be reduced to Cr(III) during the activation of sulfites for degrading pollutants [12,17,18]. The Cu(II)/Co(II)-S(IV) system can afford effective degradation under alkaline conditions [19–21], because a high pH is more conducive for the formation of Co(II)-OH/Cu(II)-OH, thus producing more $SO_x^{\bullet-}$ [2,14]. Despite these cases, the single metal-S(IV) system has the problems of pH dependency and low efficiency. Meanwhile, because $SO_4^{\bullet-}$ has high selectivity, it exhibits weak oxidizability for further mineralization, resulting in few intermediates, whereas $^{\bullet}OH$ demonstrates a satisfactory mineralization ability with excellent nonselective oxidation [20]. To solve the aforementioned problems, we introduced photocatalysis into an S(IV) system to establish a heterogeneous catalytic system because the combination of $^{\bullet}OH$ and $SO_4^{\bullet-}$ can efficiently degrade organic compounds.

TiO_2, an attractive n-type semiconductor, has become a commonly used photocatalyst because of its low price, nontoxicity, environmental protection ability, and satisfactory thermal stability [22–24]. However, its further application is retarded by ineluctable shortcomings, such as wide band gap, poor utilization of solar light, and high recombination rate of photo-generated charge carriers [25]. Therefore, it is advisable to construct a heterojunction for achieving effective charge separation and strong redox ability [26,27]. Cobalt-based materials (*e.g.*, $CoTiO_3$, CoO, Co_3O_4 and $Co(OH)_2$) can be good candidates to integrate with TiO_2 due to their intrinsic activity and low cost [4,28,29]. Co_3O_4 is a typical p-type semiconductor which exhibits a strong response to visible light and capacity of activating sodium sulfite [30,31]. Thus, compositing Co_3O_4 and TiO_2 seems to be an effective way to build advanced catalyst for photocatalytic activation of sodium sulfite.

In the present study, we constructed a heterogeneous catalytic system by using Co_3O_4 and TiO_2 nanoparticles (Co_3O_4/TiO_2) to form a p-n heterojunction that can serve as a catalyst to degrade ACE through the photocatalytic activation of sodium sulfite. This catalyst could broaden the spectrum utilization range, produce more photogenerated holes and electrons, be beneficial for charge separation, and also efficiently activate sodium sulfite. Importantly, the charge transfer from Co_3O_4 to TiO_2 was verified by X-ray photoelectron spectroscopy analysis and theoretical calculations. We investigated the effect factors of component ratios, sulfite and ACE concentrations, catalyst dosages, and initial pH on the removal efficiency of ACE. Moreover, we identified the predominant active radicals by performing radical quenching experiments and deduced the degradation pathway by monitoring generated intermediate products. The degradation mechanism for ACE removal on Co_3O_4/TiO_2 was proposed *via* photocatalytic activation of sulfite process. Our work will open up new avenues for the removal of pharmaceutical wastewater by photocatalytic activation of sulfite system, predicting the potential application value in industry.

Transmission electron microscopy (TEM) images of Co_3O_4/TiO_2 powders (Co/Ti = 1.5) with aggregating some small nanoparticles at different magnifications are shown in Figs. 1a–c to demonstrate the microstructure. The high-resolution TEM (HRTEM) image in Fig. 1c clearly displays the uniform lattice fringes of Co_3O_4 and TiO_2. The fringes with spacing of 0.203 nm correspond to (400) plane of Co_3O_4 phase (shown in the purple dashed frame) [32]. The fringe spacings with 0.351 nm as shown in the yellow part can be attributed to (101) facets of anatase TiO_2 [33]. The results indicate that the composite nanoparticles were consisted of mixed crystallites of Co_3O_4 and TiO_2. The TEM image of pure TiO_2 was shown in Fig. S1 (Supporting information). Additionally, the energy dispersive X-ray spectroscopy (EDS) element mapping images of Co_3O_4/TiO_2 indicated that Ti, Co, and O were the main elements (Fig. S2 in Supporting information). The elements composition and distribution images were performed using EDS of a selected area in Fig. 1d, indicating that three elements were distributed in the hybrid material.

The phase composition of the Co_3O_4/TiO_2 was analyzed by X-ray diffractions (XRD) in Fig. 2a. The blue line represents the XRD pattern of as-synthesized Co_3O_4 without the addition of $Ti(SO_4)_2$ in the synthesis system, which is consistent with typical Co_3O_4 (JCPDS card No. 42–1467) [34]. The diffraction peaks at 2θ of 31.27°, 36.85°, 38.54°, 44.80°, 55.65°, 59.35°, and 65.23° could be assigned to the (220), (311), (222), (400), (422), (511) and (440) crystal facets of Co_3O_4, respectively. Compared with Co_3O_4, Co_3O_4/TiO_2 (the green line in Fig. 2a) demonstrates a diffraction peak of 36.85° at 2θ, which could be assigned to the (311) crystal face of Co_3O_4 [34]. And other diffraction peaks of Co_3O_4 are ambiguous, which could be due to the relatively low crystallinity of Co_3O_4 in the hybrid materials. Besides, the residual diffraction peaks were well indexed to the JCPDS card No. 21–1272 of anatase TiO_2 [35].

Elemental composition and chemical state of Co_3O_4/TiO_2 was determined by X-ray photoelectron spectroscopy (XPS). All spectra were calibrated by C 1s with binding energy of 284.8 eV. Apparently, the survey shows Ti, O, Co, and C element characteristic peaks (Fig. 2b). High-resolution spectrum of Ti 2p in Fig. 2c is split into two spin-orbit peaks corresponding to 458.8 eV ($2p_{3/2}$) and 464.5 eV ($2p_{1/2}$), respectively which are corresponding to Ti^{4+} [36,37]. The 2p spectrum of Co in Fig. 2d shows a peak at 779.9 eV which is regarded as the characteristic peak of Co_3O_4 [38]; and the peaks at 781.1 eV and 779.9 eV were regarded as the Co^{2+} and Co^{3+} consistent with the reported Co_3O_4 [32]. As to O 1s spectrum, we have reasonably divided it into three peaks (Fig. 2e), indicating the presence of different types of oxidation species. The O1 and O2 peaks at 530.0 and 531.6 eV can be assigned to lattice oxygen of metal oxide and the hydroxyl group (Ti-OH), respectively [39,40].

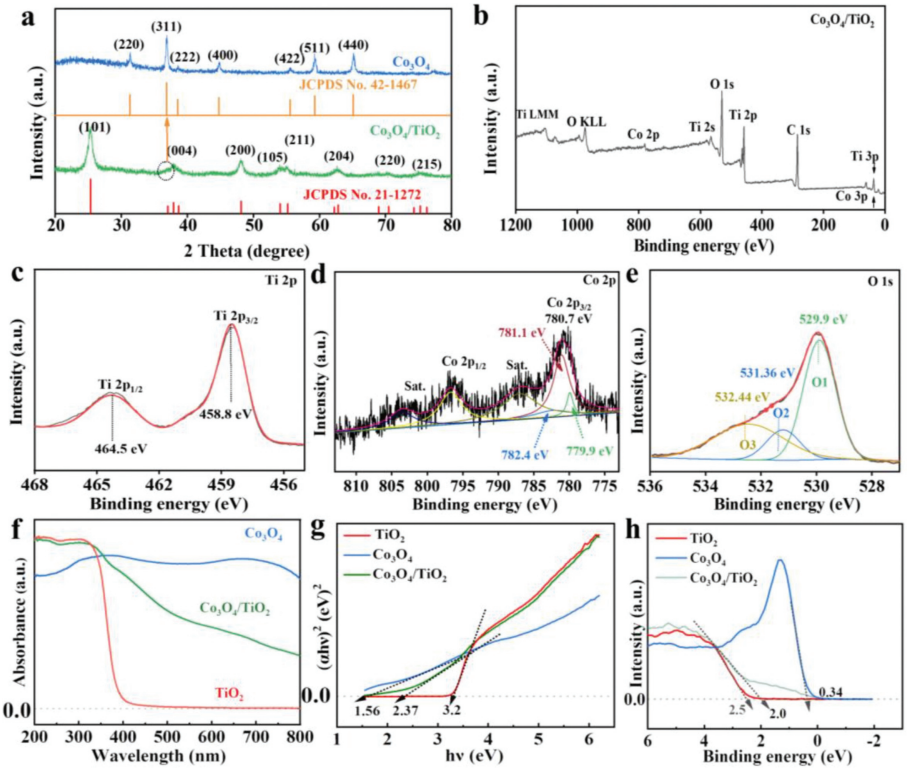

Fig. 2. (a) X-ray diffractions patterns of Co_3O_4/TiO_2 and Co_3O_4. XPS spectra of (b) full survey spectrum, (c) Ti 2p, (d) Co 2p, and (e) O 1s. (f) UV-DRS spectra of Co_3O_4/TiO_2, TiO_2 and Co_3O_4. (g) $(\alpha h\nu)^2$-$h\nu$ curve of Co_3O_4/TiO_2, TiO_2 and Co_3O_4. (h) VB-XPS spectra of Co_3O_4/TiO_2, TiO_2 and Co_3O_4.

The O 1s spectra of Co_3O_4 confirmed this result (Fig. S3 in Supporting information). The binding energy of O3 is 533.12 eV, which is assigned to adsorbed oxygen of H_2O molecules [40]. Importantly, the binding energies of Co 2p and O 1s in Co_3O_4/TiO_2 positively shifted to 1.0 eV and 0.28 eV, respectively, relative to those of Co_3O_4 (Fig. S3). These phenomena indicated the charge redistribution between Co_3O_4 and TiO_2 at the heterojunction interface [41]. The interfacial charge redistribution of Co_3O_4/TiO_2 may influenced the adsorption energies of HSO_3^- or SO_3^{2-} of sulfite activation and the catalytic activity.

The ultraviolet-visible diffused reflectance spectroscopy (UV-DRS) spectra of the synthesized materials were exhibited in Fig. 2f. The absorption wavelength in the UV region of pure TiO_2 was 387.5 nm [42], and the Co_3O_4 sample displayed an absorption wavelength in the visible-light region, which was similar with the previous studies [43]. Owing to the interfacial charge redistribution and transfer from Co_3O_4 to TiO_2, the absorption bands could widen the visible-light absorption region. In addition, the function $(\alpha h\nu)^{1/n} = A(h\nu - E_g)$ (where α is the absorption coefficient, h represents the Planck's constant, ν is the vibration frequency, E_g is the band gap, A is the proportional constant, and n is the nature of the sample transition). Owing to Co_3O_4 as the direct allowed transition material, n is 1/2, and $(\alpha h\nu)^2$ is plotted against $h\nu$ in Fig. 2g [44]. The bandgap values of the three materials were 2.37 eV for Co_3O_4/TiO_2, 3.2 eV for TiO_2, and 1.56 eV for Co_3O_4. The maximum valence band (M_{VB}) value was calculated using valence band XPS (VB-XPS) in Fig. 2h, and the M_{VB} values of Co_3O_4/TiO_2, TiO_2, and Co_3O_4 were determined to be 2.0, 2.5, and 0.34 eV, respectively.

Besides, the charge transfer path and the formation mechanism of Co_3O_4/TiO_2 heterojunction was also investigated and presented in Fig. 3. The electronic properties were calculated based on Bader charge approach *via* density functional theory (DFT) calculations [26,27]. Firstly, the work function Φ with applying to calculation of electrostatic potential in vertical direction of the monolayer was explored by the formula of $\Phi = V\infty - E_f$. Here, $V\infty$ is the vacuum potential in the vicinity of selected material, and E_f is the Fermi energy level. The computational results and values of TiO_2 and Co_3O_4 were shown in Figs. 3a and b, the calculated work functions of TiO_2 and Co_3O_4 were 3.08 and 5.598 *versus* vacuum level, respectively. One can know that when TiO_2 and Co_3O_4 form the heterostructure, the electron could flow into TiO_2 from Co_3O_4. The charge density difference in Fig. 3c also proved it. Distinctly, one can see the charge redistribution occurred at the interface of Co_3O_4/TiO_2 heterojunction. The yellow and cyan regions of the construction represented the accumulation and depletion of electrons, respectively. The planar-averaged electron density difference in Fig. 3c revealed the accumulation number of electrons. In addition, the calculated results indicated that the Co_3O_4 part near the interface displayed positively charge, while the TiO_2 part near the interface was negatively charge due to the migration of electrons. By Bader charge approach, it was found that there were electrons (2.041 e^-) transfer from Co_3O_4 to TiO_2, resulting in the electron accumulation on TiO_2 and hole accumulation on Co_3O_4, which was accord with XPS analysis. Thus, it can be concluded the heterojunction can be efficiently constructed by combining the Co_3O_4 with TiO_2.

Figs. 4a–c exhibited the kinetic data of the ACE degradation in different systems. In the absence of light, Na_2SO_3 (10 mmol/L) alone did not cause ACE degradation in 30 min. When other conditions remained unchanged, Co_3O_4 and Na_2SO_3 acted together in the system (no light), the *pseudo*-first-order rate constant (k_1) increased rapidly and the degradation efficiency increased by 69.58%, indicating that Co effectively activated sulfites [4,20]. When Co_3O_4/TiO_2 and Na_2SO_3 were simultaneously used (no light, Co_3O_4/TiO_2+S(IV), the red line), the *pseudo*-first-order reaction rate constant (k_1) increased [45], and the degradation efficiency of the pollutants was 71.66% in 30 min. This may be because the presence of Co_3O_4/TiO_2 can activate Na_2SO_3 to generate $SO_x^{\bullet-}$ [9],

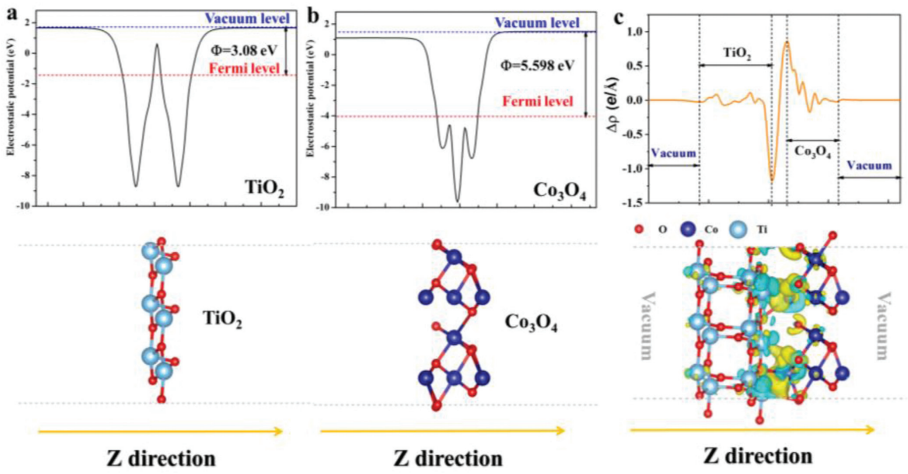

Fig. 3. The calculated work function and corresponding structural model of (a) (101) plane of TiO_2 and (b) (111) plane of Co_3O_4. (c) The planar-averaged electron density difference and side view of the charge density difference over the Co_3O_4/TiO_2 heterojunction. The yellow and cyan regions on the constructed represent accumulation and depletion of electrons, respectively.

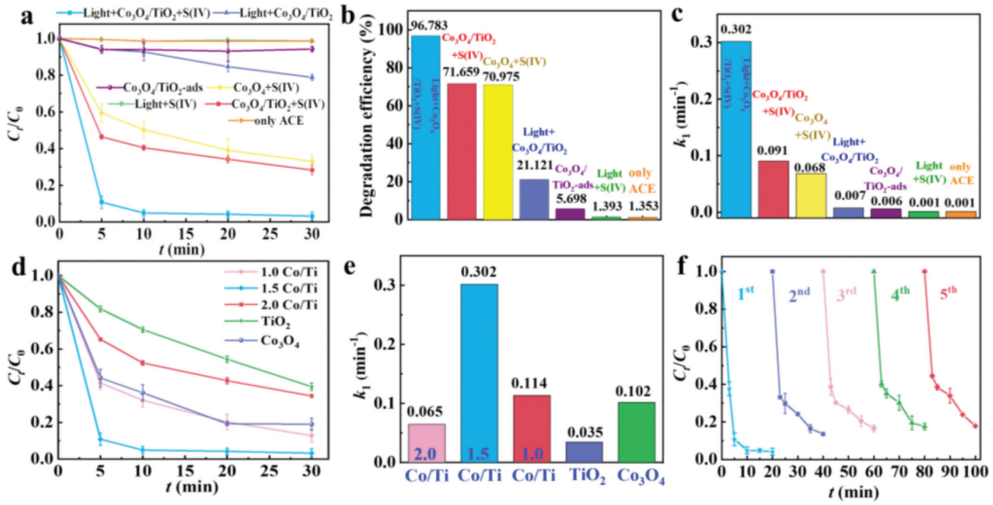

Fig. 4. (a) Effect of various processes on the degradation efficiency of ACE. (b) Degradation efficiency of various processes. (c) *Pseudo*–first-order rate constant (k_1) for ACE degradation under different systems. (d) Degradation efficiency of different catalyst under simulate solar light. (e) *Pseudo*–first-order rate constant (k_1) at different Co/Ti molar ratios. (f) ACE degradation in five continuous batch runs *via* light + Co_3O_4/TiO_2 + S(IV) system. Initial conditions: Co_3O_4/TiO_2 = 1 g/L, S(IV) = 10 mmol/L, ACE = 0.01 mmol/L, and pH 7.

thus promoting ACE degradation. In the absence of light, the adsorption efficiency of Co_3O_4/TiO_2 alone was 5.69%, indicating the weak adsorption in the system. Under illumination, Co_3O_4/TiO_2 (light + Co_3O_4/TiO_2) just removed 21.12% of the ACE in 30 min, which was lower than that the red line of Co_3O_4/TiO_2 + S(IV) (71.66%, no light). These results indicated that the degradation of ACE by $O_2^{\bullet-}$ and $^{\bullet}OH$ generated by the separation of electrons and holes in Co_3O_4/TiO_2 under light irradiation was lower than that by $SO_x^{\bullet-}$. Therefore, when Co_3O_4/TiO_2 + S(IV) under the simulate solar light illumination (Light + Co_3O_4/TiO_2 + S(IV), the blue line), the degradation efficiency significantly improved up to 96.78%. The degradation efficiency *via* photocatalytic activation of sulfite of pure Co_3O_4 and TiO_2 was lower than that of Co_3O_4/TiO_2, indicating that the composite demonstrated excellent catalytic performance.

The effect of different catalyst compositions on ACE degradation was investigated (Figs. 4d and e). The observed reaction rate constant k_1 increased first and then decreased when the Co/Ti molar ratio increased from 0 to 2, and the optimum molar ratio of Co/Ti was 1.5. The ACE removal rate by Co_3O_4/TiO_2 was better than that pure TiO_2 and Co_3O_4, indicating that hybrid structure could effectively improve catalytic performance. To examine the reusability of Co_3O_4/TiO_2 in S(IV) system, several cycle experiments were performed under optimum conditions. The degradation rate of ACE reached 80% in 20 min after five cycles in Fig. 4f, indicating that ACE still had favorable catalytic activity. However, the cyclic stability of Co_3O_4/TiO_2 decreased. This phenomenon is similar to that reported in the previous [2]. There are two reasons to explain this phenomenon: (1) Excessive ACE might occupy the active sites on the surface of catalyst to weaken the degradation performance [46]. (2) Co_3O_4/TiO_2 had the phenomenon of the metal leaching, which was contributed to shedding of the active site during the reaction process. The ICP results showed that the leaching amount of Ti^{4+} was 0.0 mg/L, but that of Co^{2+} ions was 2.0 mg/L. Table S1 (Supporting information) presented the comparison of the ACE removal efficiency under different oxidation processes, and the degradation performance of this study system was found to be superior to that of other processes. Meanwhile, the effect of pH, role of Na_2SO_3, dosage of catalyst, ACE concentration, influence of natural anions, and total organic carbon can be seen in Text S3 and Figs. S4–S7 (Supporting information).

To elucidate the underlying mechanism for the photocatalytic activation of sulfite degradation of ACE, we added different

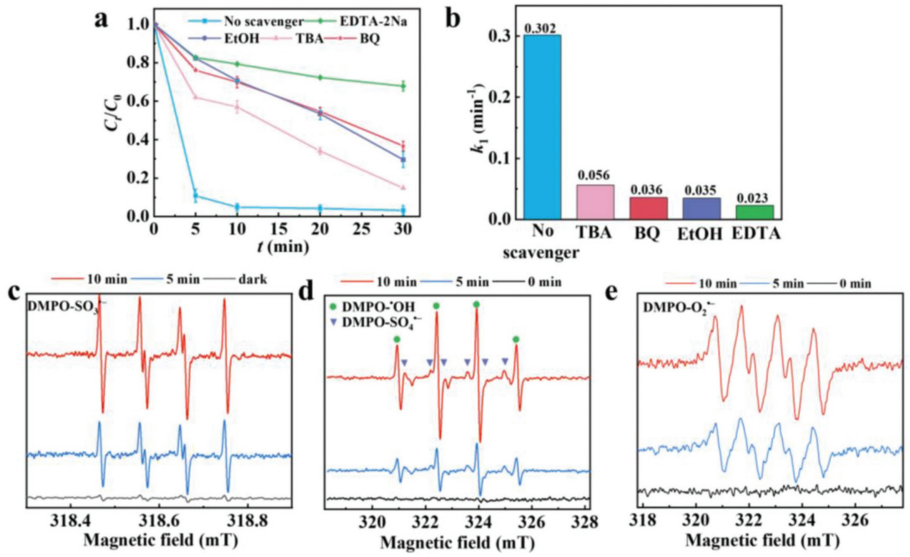

Fig. 5. (a) Inhibition effects of radical scavengers on the degradation of ACE, [EtOH] = 10 mmol/L, [TBA] = 10 mmol/L, [BQ] = 1 mmol/L, [EDTA-2Na] = 1 mmol/L. (b) *Pseudo*-first-order rate constant (k_1) for the degradation of ACE under different quenching agents. (c) ESR spectra of DMPO-$SO_3^{\bullet-}$ in a nitrogen atmosphere under dark or light conditions. (d) ESR spectra of DMPO-$^{\bullet}OH$ and DMPO-$SO_4^{\bullet-}$ at different reaction times under light conditions. (e) ESR spectra of DMPO-$O_2^{\bullet-}$ at different reaction times, V_L:V_{DMSO} = 1:1 (V_L is the sampling volume of reaction solution). Initial conditions: Co_3O_4/TiO_2 = 1 g/L, S(IV) = 10 mmol/L, pH 7, DMPO = 100 mmol/L, no stirring, and exposed to air.

quenchers to perform scavenging experiments to identify the primary active radicals as described in Figs. 5a and b. On the basis of the findings of previous studies, we used *tert*–butanol (TBA) and benzoquinone (BQ) as the scavengers of $^{\bullet}OH$ and $O_2^{\bullet-}$, respectively. Ethanol (EtOH) can act as a scavenger of $^{\bullet}OH$ as well as react with $SO_4^{\bullet-}$ [2,47]. The addition of TBA, BQ, and EtOH resulted in 14.78%, 36.74%, and 29.6% reductions in ACE degradation efficiency, indicating that species containing $^{\bullet}OH$, $O_2^{\bullet-}$, and $SO_4^{\bullet-}$ were generated in the light+Co_3O_4/TiO_2+*S*(IV) system. After addition of ethylenediaminetetraacetic acid disodium salt (EDTA-2Na) (as a quencher for h^+), the ACE degradation efficiency significantly decreased from 96.78% to 32.17%. The above results deduced that $^{\bullet}OH$, h^+, and $SO_x^{\bullet-}$ played vital roles in the degradation of ACE. Particularly, $SO_3^{\bullet-}$ could be generated by Co_3O_4/TiO_2 through photocatalytic activation of sulfite process.

ESR was performed to detect the generation of free radicals in the light+Co_3O_4/TiO_2+S(IV) system with 5,5-dimethyl-1-pyrroline N-oxide (DMPO) as the capture agent. Fig. 5c displayed the ESR spectra under dark or light conditions and nitrogen purge conditions. A weak signal was detected in the dark, and the peak of DMPO-$SO_3^{\bullet-}$ was observed under light condition [2,48]. The peak intensity increased with an increase in the duration of light irradiation, which may be attributable to $^{\bullet}OH$ and $SO_3^{\bullet-}$. Fig. 5d displayed the ESR spectra of exposed air under light conditions, and the peaks of DMPO-$^{\bullet}OH$ (the hyperfine coupling constants of $aN = 1.488$ mT and $aH = 1.488$ mT) [49] and DMPO-$SO_4^{\bullet-}$ ($aN = 1.417$ mT, $a_\beta H = 0.966$ mT, $a_\beta H = 0.117$ mT, and $a_\gamma H = 0.078$ mT) were observed [46,50]. In the presence of DMSO, $O_2^{\bullet-}$ with the hyperfine coupling constants of $aN = 1.371$ mT, $a_\beta H = 1.005$ mT, and $a_\gamma H = 0.32$ mT was found in Fig. 5e [51]. The results of ESR were in favorable agreement with those of free radical capture experiments. In addition, we also used furfuryl alcohol (FFA) as the scavenger of singlet oxygen ($^1O_2$). The quenching test indicated that the addition of FFA could not inhibit the degradation of ACE. Therefore, we conclude that $^1O_2$ does not play a role in the light + Co_3O_4/TiO_2 + S(IV) system. And the ESR results showed that there was no signal of $^1O_2$ in the system as shown in Fig. S8 (Supporting information). In conclusion, $^{\bullet}OH$, h^+ and $SO_x^{\bullet-}$ may be the main active species in the degradation process. In addition, the possible removal pathways were proposed in Text S4, Table S2, and Fig. S9 (Supporting information).

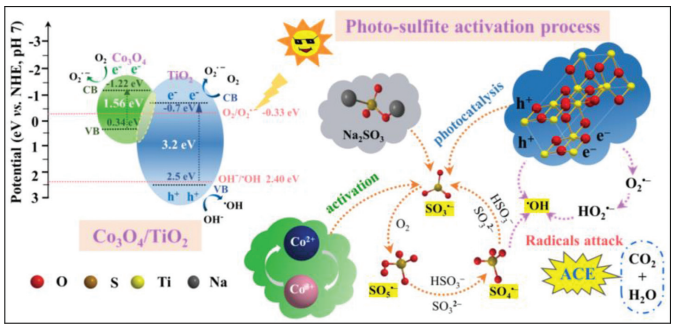

Scheme 1. Degradation mechanism of the Co_3O_4/TiO_2 through the photocatalytic activation of sulfite process.

Finally, the ACE removal mechanism by using Co_3O_4/TiO_2 as catalysts *via* photocatalytic activation of sulfite was proposed according to the XPS analysis and Bader charge approach, which might be due to two aspects: (1) The heterojunction structure can broaden the utilized spectrum range, produce more photogenerated holes and electrons, and facilitate charge separation (Eqs. 1 and 2). The charge transfers induced electron accumulation on TiO_2 near the interface readily react with O_2 molecules to generate more $O_2^{\bullet-}$ (Eq. 3). And the $O_2^{\bullet-}$ and h^+ further react with H_2O or OH to generate $^{\bullet}OH$ (Eqs. 4 and 5). The rapid depletion of electrons could stimulate the generation of more holes in the valence band under light illumination, which could react with SO_3^{2-} to produce more $SO_x^{\bullet-}$ (Eqs. 6–9) [2,14]. (2) Noticeably, the positively charged Co_3O_4 at interface was beneficial for the adsorption of HSO_3^- or SO_3^{2-} to generate reactive species (*i.e.*, $SO_3^{\bullet-}$, $SO_4^{\bullet-}$, $SO_5^{\bullet-}$) and further promoted sulfite activation performance.

On the basis of the aforementioned results, the reaction mechanism of the light + Co_3O_4/TiO_2 + S(IV) system was deduced as follows (Scheme 1). When Co_3O_4/TiO_2 was added to the system, h^+ and e^- were photogenerated on the surface excited by light illumination, and a series of active substances were directly or indirectly generated by the action of O_2 and H_2O in the solution (Eqs. 1–5) [23,52]. A series of chain reactions of sulfite could generate $SO_x^{\bullet-}$, such as light excitation (Eq. 6) [53,54] or direct or indirect reaction with h^+ or $^{\bullet}OH$ (Eqs. 7–13) [9,13,23]. Under alkaline condi-

tions, complexation occurred on the surface (Eqs. 14–17) [2,20]. Finally, a series of reactive radicals were generated that could improve the photocatalytic activation of sulfite performance and degrade organic compounds. All equations can be observed as following parts (Eqs. 1–17).

$$TiO_2 + h\nu \rightarrow e^- + h^+ \quad (1)$$

$$Co_3O_4 + h\nu \rightarrow e^- + h^+ \quad (2)$$

$$e^- + O_2 \rightarrow O_2^{\bullet-} \quad (3)$$

$$O_2^{\bullet-} + H_2O \rightarrow HO_2^{\bullet-} + {}^{\bullet}OH \quad (4)$$

$$h^+ + OH^- \rightarrow {}^{\bullet}OH \quad (5)$$

$$SO_3^{2-} + h\nu \rightarrow e^- + SO_3^{\bullet-} \quad (6)$$

$$SO_3^{2-} + h^+ \rightarrow SO_3^{\bullet-} \quad (7)$$

$$SO_3^{2-} + {}^{\bullet}OH \rightarrow OH^- + SO_3^{\bullet-} \quad (8)$$

$$SO_3^{\bullet-} + O_2 \rightarrow SO_5^{\bullet-} \quad (9)$$

$$SO_5^{\bullet-} + HSO_3^- \rightarrow HSO_4^- + SO_4^{\bullet-} \quad (10)$$

$$SO_5^{\bullet-} + SO_3^{2-} \rightarrow SO_4^{2-} + SO_4^{\bullet-} \quad (11)$$

$$SO_4^{\bullet-} + HSO_3^- \rightarrow HSO_4^- + SO_3^{\bullet-} \quad (12)$$

$$SO_4^{\bullet-} + SO_3^{2-} \rightarrow SO_4^{2-} + SO_3^{\bullet-} \quad (13)$$

$$Co(II) + H_2O \rightarrow Co(II)\text{–}OH\ (\text{alkaline}) \quad (14)$$

$$Co(II)\text{–}OH + SO_3^{2-} \rightarrow Co(II)\text{–}SO_3 + H_2O \quad (15)$$

$$Co(II)\text{–}SO_3 + O_2 \rightarrow Co(III)\text{–}SO_3^+ \quad (16)$$

$$Co(III)\text{–}SO_3^+ + SO_3^{2-} \rightarrow Co(II)\text{–}SO_3 + SO_3^{\bullet-} \quad (17)$$

We constructed a heterogeneous system involving Co_3O_4 and TiO_2 nanoparticles to form the p-n heterojunction interface as an efficient catalyst for degrading ACE through photocatalytic activation of sulfite. This catalyst could broaden the utilized spectrum range, produce more photogenerated holes and electrons, facilitate charge separation, and activate sulfite. Charge transfers induced electron accumulation on TiO_2 and hole accumulation on Co_3O_4 were verified by XPS analysis and DFT calculations. Optimal catalytic efficiency could reach 96.78% within 10 min based on the systematic study on experimental parameters (*i.e.*, ACE and sulfite concentrations, catalyst ratio, catalyst dosage, and initial pH). We identified the predominant active radicals by performing radical quenching experiments and using the ESR capture technique which indicated that $^{\bullet}OH$, h^+, and $SO_x^{\bullet-}$ were the main active species. The stability and recyclability of Co_3O_4/TiO_2 are confirmed by performing cycling tests. And the degradation pathway is determined by monitoring the generation of intermediate products. Finally, we propose the degradation mechanism of ACE by Co_3O_4/TiO_2 *via* photocatalytic activation of sulfite. Our work provides a new strategy to design efficient catalyst by engineering heterointerface for sulfite oxidation, which could guide the construction of catalysts. The high-efficient photocatalytic activation system could effectively utilize sulfite to degrade organic pollutants, predicting potential industrial applications for the removal of pharmaceutical wastewater.

Declaration of competing interest

The authors declare that they have no known competing financial interests or personal relationships that could have appeared to influence the work reported in this paper.

Acknowledgments

This work was financially supported by the National Natural Science Foundation of China (No. 51878273) and the Natural Science Foundation of Hebei Province (No. E2019502199).

Supplementary materials

Supplementary material associated with this article can be found, in the online version, at doi:10.1016/j.cclet.2022.05.044.

References

[1] D. Guo, S. You, F. Li, Y. Liu, Chin. Chem. Lett. 33 (2022) 1–10.
[2] T. Luo, Y. Yuan, D. Zhou, et al., Chem. Eng. J. 363 (2019) 329–336.
[3] J. Qi, J. Liu, F. Sun, et al., Chin. Chem. Lett. 32 (2021) 1814–1818.
[4] P. Hu, M. Long, Appl. Catal. B 181 (2016) 103–117.
[5] M. Ma, L. Chen, J. Zhao, W. Liu, H. Ji, Chin. Chem. Lett. 30 (2019) 2191–2195.
[6] X. Lei, M. You, F. Pan, et al., Chin. Chem. Lett. 30 (2019) 2216–2220.
[7] J. Li, Y.J. Li, Z.K. Xiong, et al., Chin. Chem. Lett. 30 (2019) 2139–2146.
[8] L. Chen, M. Tang, C. Chen, et al., Environ. Sci. Technol. 51 (2017) 12663–12671.
[9] W. Deng, H. Zhao, F. Pan, et al., Environ. Sci. Technol. 51 (2017) 13372–13379.
[10] R. Dewil, D. Mantzavinos, I. Poulios, M.A. Rodrigo, J. Environ. Manag. 195 (2017) 93–99.
[11] Z. Wang, F. Bai, L. Cao, et al., Chin. Chem. Lett. 33 (2022) 4766–4770.
[12] H. Dong, G. Wei, W. Fan, et al., Chemosphere 196 (2018) 593–597.
[13] L. Chen, X. Peng, J. Liu, J. Li, F. Wu, Ind. Eng. Chem. Res. 51 (2012) 13632–13638.
[14] D. Zhou, L. Chen, J. Li, F. Wu, Chem. Eng. J. 346 (2018) 726–738.
[15] P. Xie, Y. Guo, Y. Chen, et al., Chem. Eng. J. 314 (2017) 240–248.
[16] Y. Yuan, S. Yang, D. Zhou, F. Wu, J. Hazard. Mater. 307 (2016) 294–301.
[17] B. Jiang, S. Xin, Y. Liu, et al., J. Hazard. Mater. 343 (2018) 1–9.
[18] B. Jiang, X. Wang, Y. Liu, et al., J. Hazard. Mater. 304 (2016) 457–466.
[19] L. Chen, T. Luo, S. Yang, et al., Environ. Chem. Lett. 16 (2018) 599–603.
[20] Y. Yuan, D. Zhao, J. Li, et al., Catal. Today 313 (2018) 155–160.
[21] Z. Liu, S. Yang, Y. Yuan, et al., J. Hazard. Mater. 324 (2017) 583–592.
[22] Q. Pang, G. Liao, X. Hu, Q. Zhang, Z. Xu, J. Inorg. Mater. 34 (2019) 219–224.
[23] V. Vaiano, O. Sacco, M. Matarangolo, Catal. Today 315 (2018) 230–236.
[24] Q. Li, Y. Liu, Z. Wan, et al., Chin. Chem. Lett. 33 (2022) 3835–3841.
[25] Z. Wang, Z. Lin, S. Shen, W. Zhong, S. Cao, Chin. J. Catal. 42 (2021) 710–730.
[26] P. Xia, S. Cao, B. Zhu, et al., Angew. Chem. Int. Ed. 59 (2020) 5218–5225.
[27] J. Qi, X. Yang, P. Pan, et al., Environ. Sci. Technol. 56 (2022) 5200–5212.
[28] H. Wang, Q. Gao, H. Li, et al., Chem. Eng. J. 368 (2019) 377–389.
[29] H. Li, Q. Gao, G. Wang, et al., Chem. Eng. J. 392 (2020) 123819.
[30] I. Rabani, R. Zafar, K. Subalakshmi, et al., J. Hazard. Mater. 407 (2021) 124360.
[31] H. Zhang, J. Wang, X. Zhang, B. Li, X. Cheng, Chem. Eng. J. 369 (2019) 834–844.
[32] L. Xu, Q. Jiang, Z. Xiao, Angew. Chem. Int. Ed. 55 (2016) 5277–5281.
[33] S. Liu, J. Huang, L. Cao, et al., Mater. Sci. Semicond. Proc. 25 (2014) 106–111.
[34] J. Zhong, A. Wang, G. Li, et al., J. Mater. Chem. A 22 (2012) 5656–5665.
[35] Q. Wang, Y. Cui, R. Huang, et al., Chem. Eng. J. 383 (2020) 123142.
[36] Y. Shieh, Y. Chang, Thin Solid. Films 518 (2010) 7464–7467.
[37] R. Tang, S. Zhou, Z. Yuan, L. Yin, Adv. Funct. Mater. 27 (2017) 1701102.
[38] J. Yang, H. Liu, W.N. Martens, R.L. Frost, J. Phy. Chem. C 114 (2010) 111–119.
[39] Q. Yang, H. Choi, D.D. Dionysiou, Appl. Catal. B 74 (2007) 170–178.
[40] X. Dong, B. Ren, X. Zhang, et al., Appl. Catal. B 272 (2020) 118971.
[41] G. Yang, Y. Jiao, H. Yan, Adv. Mater. 32 (2020) 2000455.
[42] M. Anpo, M. Takeuchi, J. Catal. 216 (2003) 505–516.
[43] D. Barreca, C. Massignan, S. Daolio, et al., Chem. Mater. 13 (2001) 588–593.
[44] C. Gao, Q. Meng, K. Zhao, et al., Adv. Mater. 28 (2016) 6485–6490.
[45] Q. Chen, L. Chen, J. Qi, et al., Chin. Chem. Lett. 30 (2019) 1214–1218.
[46] X. Tao, P. Pan, T. Huang, et al., Chem. Eng. J. 395 (2020) 125186.
[47] S. Guo, H. Tang, L. You, et al., Chin. Chem. Lett. 32 (2021) 2828–2832.
[48] F. Chen, Q. Yang, F. Yao, et al., Chem. Eng. J. 355 (2019) 624–636.
[49] Y. Wang, S. Indrawirawan, X. Duan, Chem. Eng. J. 266 (2015) 12–20.
[50] Y. Chen, G. Zhang, H. Liu, J. Qu, Angew. Chem. Int. Ed. 58 (2019) 8134–8138.
[51] C. Diaz-Uribe, M. Daza, F. Martinez, J. Photochem. Photobiol. A 215 (2010) 172–178.
[52] L. Yang, L.E. Yu, M.B. Ray, Water Res. 42 (2008) 3480–3488.
[53] X. Yu, D. Cabooter, R. Dewil, Sci. Total Environ. 688 (2019) 65–74.
[54] M. Entezari, H. Godini, A. Sheikhmohammadi, A. Esrafili, J. Water Process Eng. 32 (2019) 100983.